

Development of Bearing Fault Detection Models using Multibody Simulation Training Data

Luca Giraudo¹, Luigi Gianpio Di Maggio², Eugenio Brusa³, and Cristiana Delprete⁴

^{1,2,3,4} *Department of Mechanical and Aerospace Engineering, Politecnico di Torino, 10129, Italy*

luca.giraudo@polito.it

luigi.dimaggio@polito.it

eugenio.brusa@polito.it

cristiana.delprete@polito.it

ABSTRACT

This study evaluates the performance of simulation-trained fault detection models on large spherical roller bearings vibration data. A high-fidelity multibody (MB) model of a SKF 22240 CCK/W33 bearing is developed through Simscape Multibody to reproduce the coupled dynamics of inner and outer rings, cage, and 38 rolling elements. Localized defects on raceways are represented through a point-cloud contact formulation, where selected nodes are radially displaced to emulate faults. The model outputs triaxial accelerations at the outer ring under realistic loading and speed conditions that mirror an experimental test campaign. Simulation signals are processed through bandpass filtering, envelope analysis, and segmentation. A set of 23 time and frequency domain features is extracted from each segment, then each feature vector is normalized. The same processing chain is applied to experimental data acquired on a medium-to-large bearing test rig at Politecnico di Torino, mounting SKF 22240 CCK/W33 bearings with machined inner race, outer race, and rolling element defects. A supervised Artificial Neural Network (ANN) classifier is trained only on the simulated feature dataset and then directly evaluated on the independent experimental dataset, in a process free of any data transfer. The network addresses a two-class problem (healthy and damaged), and its performance is assessed through standard classification metrics computed over multiple bootstraps of both training and test sets. Despite the intrinsic differences between simulated and experimental signals, the ANN trained purely on simulations provides reliable and selective fault detection on real measurements. Most residual classification errors are concentrated in low-speed inner race damage conditions, where fault signatures are weak and partially overlap with healthy observations, while high-speed and outer race

damage conditions are recognized more robustly. These results show that MB simulation can generate sufficiently realistic vibration data to train ANN-based fault detection models that generalize experimental measurements for large spherical roller bearings. The proposed framework introduces an alternative to costly fault campaigns and offers a flexible way to expand training datasets across loads, speeds, and defect sizes in industrial condition monitoring applications.

1. INTRODUCTION

Intelligent Fault Diagnosis (IFD) of rotating machinery, often based on vibration signals from rolling element bearings (REBs), supports early fault detection and enables predictive maintenance (Surucu, Gadsden, & Yawney, 2023; Lei et al., 2020). In parallel, Machine Learning (ML) methods for vibration-based diagnosis have rapidly expanded, supported by publicly available benchmark datasets (Widodo & Yang, 2007; Smith & Randall, 2015).

Despite high reported accuracies, most approaches remain strongly tied to the operating conditions represented in the training data. In practice, vibration signatures are highly sensitive to load, speed, assembly, and other boundary conditions, so distribution shifts between training and deployment can severely reduce robustness and transferability (Antoni, 2021; Lei, Jia, Lin, Xing, & Ding, 2016).

To address these limitations, a large body of work has explored Transfer Learning (TL) and domain adaptation strategies (Pan & Yang, 2010; Traganitis & Strangas, 2023). Recent approaches include adversarial and multistage architectures and other deep domain adaptation methods, which have shown promising results across operating regimes and machines (Zhu, Wang, Peng, & Li, 2021; Zhou, Zheng, Wang, & Gogu, 2020). Nevertheless, these methods often still require experimental data from the target domain for calibration or validation, which can be expensive and difficult to acquire in industrial contexts (Misbah, Lee, & Keung, 2024; Tang, Ma,

Luca Giraudo et al. This is an open-access article distributed under the terms of the Creative Commons Attribution 3.0 United States License, which permits unrestricted use, distribution, and reproduction in any medium, provided the original author and source are credited.

Yan, Zhu, & Khoo, 2024).

An alternative direction is simulation-driven training, where synthetic vibration data are generated to support model development. Classical studies relied on analytical bearing models with localized defects (McFadden & Smith, 1984; D. Wang, Tse, & Tsui, 2013; Sobie, Freitas, & Nicolai, 2018), while finite element (FE) models can generate richer signals but at a high computational cost (T. Wang et al., 2023; Zhao, Zhang, Wang, & Peng, 2023). More recently, simulation has been combined with TL and generative approaches to reduce discrepancies between simulated and experimental domains (C. Liu & Gryllias, 2022; X. Liu, Liu, Xiang, & Sun, 2023). However, these methods still require careful tuning and do not fully capture the variety of cases encountered in practice.

Multibody (MB) modeling has emerged as a promising compromise between physical fidelity and computational cost. Vehviläinen et al. (Vehviläinen et al., 2024) used an MB bearing model with different simulated damages to train ML classifiers, but validation against experimental measurements remains limited. Moreover, simulation-driven fault detection of large spherical roller bearings (SRBs) is still scarcely addressed despite their widespread industrial use.

Building on this gap, this study leverages the dynamic MB model proposed in (Giraud, Di Maggio, Giorio, & Delprete, 2025) to generate a simulated training dataset aimed at achieving reliable performance on experimental data. An ANN classifier is trained exclusively on simulated features and then evaluated on independent experimental measurements without any domain adaptation, to assess the feasibility of simulation-only training under realistic operating conditions.

2. METHODS

2.1. Experimental setup and data

The experimental signals used in this study come from a benchmark dataset collected on a medium-to-large bearing test rig at Politecnico di Torino (Brusa, Delprete, Giorio, Di Maggio, & Zanella, 2022; Di Maggio, Giorio, Delprete, & Brusa, 2024). The rig enables independent adjustment of radial load, axial load, and shaft rotational speed, allowing vibration measurements to be acquired in a controlled and repeatable way under operating conditions representative of industrial practice. An overview of the rig and its main components is reported in Figure 1.

The reference dataset (Di Maggio et al., 2024) contains vibration recordings for four health conditions of the SKF® 22240 CCK/W33 bearing: healthy (H), inner-race defect (IR), outer-race defect (OR), and rolling-element defect (B). Localized faults were introduced by machining pits with a diameter of 2 mm and a depth of 0.5 mm on the most heavily loaded region of the raceway under axial loading, as shown in Figure 2. While these artificial defects do not represent the full range

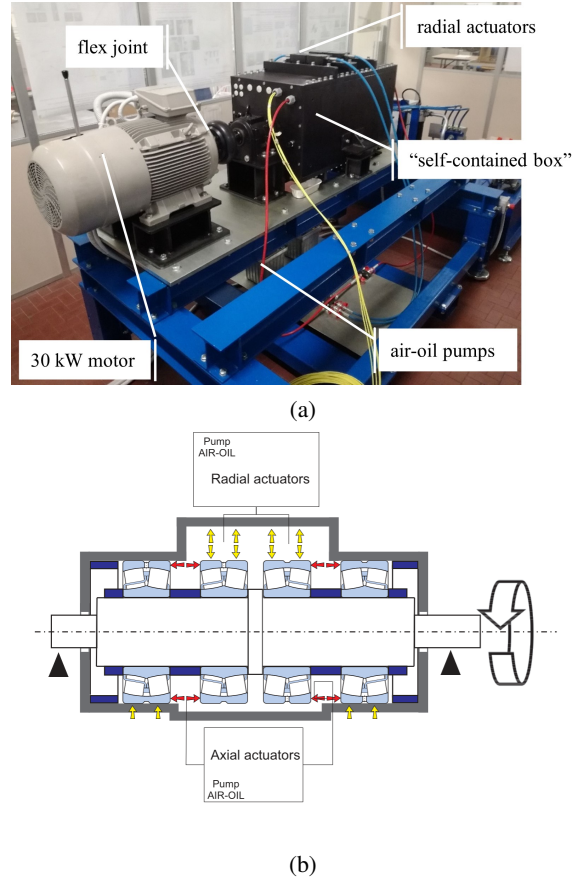


Figure 1. Test rig for condition monitoring of medium-size bearings: (a) self-contained box, (b) load path.

of damage mechanisms encountered in service, they provide a repeatable and well-defined benchmark for studying localized fault signatures. The selected defect dimensions are consistent with evidence observed in bearings returned from service by the manufacturer, but they are closer to the lower bound of the sizes typically reported. This choice is intended to assess whether the monitoring approach can detect damage at an early stage from the measured dynamic response.

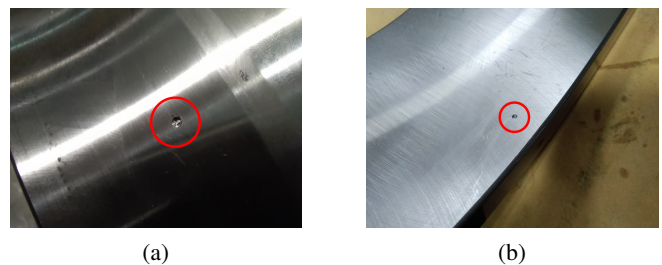


Figure 2. Localized damage: (a) IR damage, (b) OR damage.

Acceleration measurements were acquired through SKF® CMSS 2200T accelerometers, mounted on the bearing supports, sampled at 20480 Hz. Each experimental acquisition lasts ap-

proximately 60 s. For the purposes of this work, experimental runs were selected by limiting rotational speed and load so as to match the simulated operating conditions summarized in Table 1, discussed in the following paragraph. From the possible four bearings mounted on the rig, the acceleration signal from the damaged bearing was used.

2.2. Bearing modeling

The simulated signals were generated using the MB model of the SKF® 22240 CCK/W33 spherical roller bearing presented in (Giraudo et al., 2025), implemented in Simulink® through the Simscape Multibody library. The model accounts for the dynamics of the inner and outer rings, the cage, and 38 rolling elements. The simulation provides the outer-ring acceleration, which is regarded as the simulated counterpart of the accelerometer measurement. An overview of the MB model is shown in Figure 3.

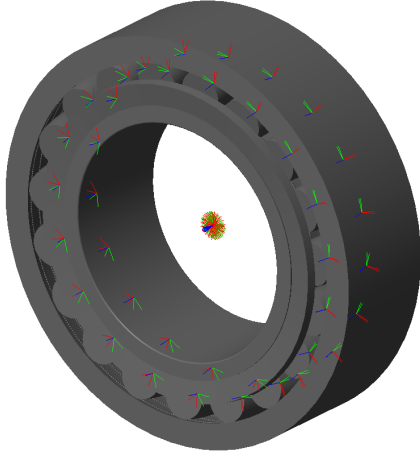


Figure 3. Multibody model of the SKF® 22240 CCK/W33 bearing implemented in Simulink® Simscape Multibody.

Rolling-element to raceway contact forces are evaluated using a penalty method based on the point-cloud representation of the raceway profiles. Simulations were carried out for nine inner-ring speeds and one external load condition. Owing to the current contact-model implementation, only inner-race and outer-race localized defects, together with the healthy condition, could be simulated. The operating parameters are reported in Table 1. External load is simulated as radial only at a constant 124.8 kN. Each simulation is calculated using an explicit RK4 solver at a fixed $1.6276 \cdot 10^{-5}$ s timestep.

The signals used in this work are limited to the IR, OR and H conditions. Rolling-element defects were not included in the present analysis because the current simulation contact-model implementation is not validated for rolling element faults; extending it to rolling-element defects is left to future work. The damaged conditions are aggregated in a single class, equally named and hereafter referred as (D).

Table 1. Inner-ring speed and external load used in the simulations.

Radial load (kN)	124.8
Axial load (kN)	0
Inner ring speed (rpm)	120, 340, 443, 508, 591, 710, 859, 920, 980

2.3. Signal preprocessing

Time signals are band-pass filtered at 1000-2500 Hz. This range was selected using only the simulated data and then applied unchanged to the experimental data, to prevent tuning preprocessing parameters on the test set. This procedure is possible since the simulated data is available in its completeness before training.

Subsequently the signal's envelope was calculated using the Hilbert transform. By observing the envelopes in Figure 4 the similarity between the two signals is evident. Even though the real data of Figure 4 (a) presents duller, less regular peaks than the simulated ones (Figure 4 (b)), the two signals present the same pattern of modulation typical of IR localized faults. For a more in-depth analysis of the datasets, the reader is referred to (Di Maggio et al., 2024) and (Giraudo et al., 2025).

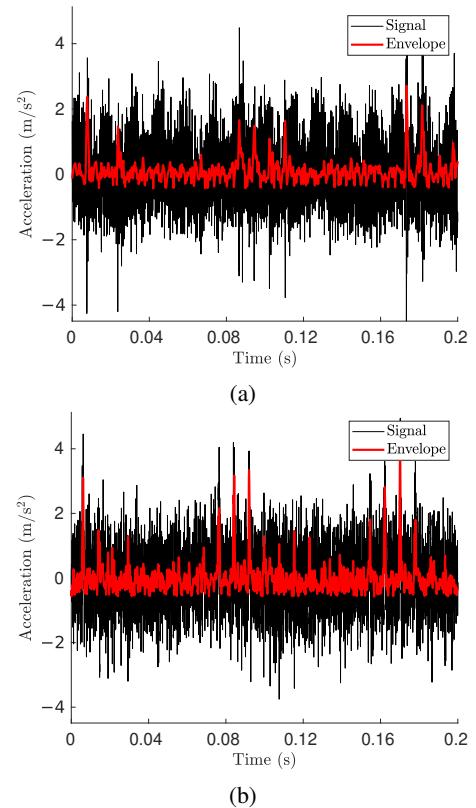


Figure 4. Normalized signal and its after-filtering envelope of the acceleration run at 710 rpm with a 128 kN radial load, IR fault: (a) Experimental, (b) simulated (Giraudo et al., 2025).

Enveloped signals are then segmented into multiple samples of approximately 1.2 s, with an overlap of 67%. From each sample a set of 23 time and frequency features is calculated. The functions used are taken from (Lei, He, Zi, & Hu, 2007) and are reported in the appendix. Finally, each feature is standardized column-wise by subtracting its mean and dividing by its standard deviation. Normalization is performed independently for the simulated and experimental datasets. Table 2 summarizes the characteristics of the obtained datasets.

Table 2. Key features of the simulated and experimental datasets.

	Simulated	Experimental
Length	697	3851
n. of Predictors	23	
Length of Time samples	1.225 s	
Positive (D) Samples	492	2438
Negative (H) Samples	205	1413
Shaft mean rotational speeds (rpm)	120, 340, 443, 508, 591, 710, 859, 920, 980	
Radial load (kN)	124.8	
Axial load (kN)	0	

2.4. Neural network parameters

This section describes the baseline architecture adopted for the ANNs. Each model is a feed-forward network composed of three fully connected hidden layers followed by a softmax output layer. The hidden-layer widths are 3, 4, and 2 neurons, respectively. Wider and deeper networks achieved comparable performance but did not yield considerable improvements on the experimental test set; therefore, the smallest stable architecture was retained.

This architecture was selected with the help of a Bayesian optimization procedure to identify the best-performing hyperparameter configuration. The optimization objective was to minimize a cost-sensitive classification criterion, evaluated on the complete training dataset using five fold cross validation. The search space constrained the network depth to a maximum of five hidden layers and the width of each hidden layer to between 1 and 300 neurons, and it also included the activation function, the learning rate, and the weight and bias initialization strategy. Within this search, the hyperbolic tangent activation provided the most stable behaviour and was therefore retained in the final model, while the alternative candidate activations were ReLU, sigmoid, and linear. The specifics of the optimizer mechanics are omitted for brevity,

several top-ranked configurations were additionally retrained and re-evaluated, confirming consistent performance trends.

2.5. Testing methodology

To assess the sensitivity of the metrics, reported in the results, to the specific data realization, a bootstrapping procedure was adopted for both the simulated training set and the experimental test set. The simulated dataset was resampled with replacement to generate multiple training replicates, each used to train an independent classifier. In parallel, the experimental dataset was resampled with replacement to generate multiple test replicates. Performance metrics were computed across all training–test bootstrap combinations and reported as averages with percentile intervals, verifying that the conclusions are not dominated by any single resampled dataset. A total of 100 models were trained, each was tested on 100 different versions of the experimental dataset.

Presented in the next section are the testing results, which were aggregated across all testing and training iterations.

3. RESULTS

Bootstrapping was applied to both the simulated and experimental datasets to create a sufficiently large statistical base of results. The aggregated outcomes of the cross-classification can be observed in Figure 5. Here, the classification results of each NN, across both sim and experimental bootstraps, are summed together to be then represented in a Confusion Matrix (CM). The top CM, presenting row-normalized values, shows that 8.8% of healthy samples are incorrectly classified as damaged, while 15.5% of damaged samples are misclassified as healthy. The bottom matrix displays the column-normalized values, which reports a 5.7% incidence of false positives, whereas 22.6% of samples predicted as healthy are actually damaged, indicating that the dominant error mode is false negatives.

To further study the resulting classification, the scores obtained from the last softmax layer are presented in Figure 6, divided in two graphs by the actual class. As can be seen in 6 (a) there is a clear performance drop for low speed classes. Here, the scores for the two classes show lack of confidence, while for higher speed values, the classification is certain. This is attributed to the low vibrational energy, generated by the passage of rolling elements on the faults, at low speeds. For these cases, feature-based classification could be insufficient at highlighting the damage signatures. Some classification uncertainty is also present for the 727 rpm speed, where outliers can be seen occupy the entire score scale. A possible explanation is that a few samples contained a localized event that lowered the signal to noise ratio, that then got repeated multiple times due to the bootstrapping. Figure 6 (b) mirrors the findings of the confusion matrix, with a slight trend of reduction of the certainty margin by growing speed. This



Figure 5. Aggregated classification results, top row-normalized Confusion Matrix and bottom column normalized values.

behavior can be associated to the growth of the vibrational effects at higher spin speeds, which fouls the healthy samples making them similar to the damaged ones, a condition which the simulated model does not seem to be able to replicate.

Table 3 reports the mean classification metrics obtained from bootstrapping and the respective 95th percentiles from all iterations, training and testing both. Specificity and precision stand above 90% while recall suffers from the false negatives discussed in the previous section. The 95th percentiles of recall deviate from the mean by less than $\pm 5\%$. This result displays the consistency of the methodology in training and testing both, showing the stability of the models trained on simulated dataset.

Table 3. Mean classification results and 95th percentiles across all learners for the classification of the experimental dataset.

	Specificity	Recall	Precision
Val.	97.5% 2.5%	84.49% 86.10% 82.40%	94.28% 96.93% 92.27%

4. CONCLUSION

In this work simulation-based training for fault detection models was explored. The acceleration signals retrieved from a MB model of a REB were used to train ANNs then used to classify real data. The resulting metrics show great quality in the classification, highlighting the clear correlation between the two data sources. The idea behind this paper sets the base for an alternative route to traditional experimental-only methods, for fault detection. The framework used in this paper will be used and improved on in future works. More complex Neural Network types will be used to classify acceleration

signals directly, thus avoiding most preprocessing. Moreover, not relying on feature-based detection will help improve performance where statistical predictors show little variance between damaged and healthy cases. On the dataset’s side, the modeling of REBs will be expanded both on physical phenomena and bearing models.

REFERENCES

Antoni, J. (2021, June). A Critical Overview of the “Filterbank-Feature-Decision” Methodology in Machine Condition Monitoring. *Acoustics Australia*, 49(2), 177–184. doi: 10.1007/s40857-021-00232-7

Brusa, E., Delprete, C., Giorio, L., Di Maggio, L. G., & Zanella, V. (2022). Design of an Innovative Test Rig for Industrial Bearing Monitoring with Self-Balancing Layout. *Machines*, 10(54). doi: 10.3390/machines10010054

Di Maggio, L. G., Giorio, L., Delprete, C., & Brusa, E. (2024, October). *Dataset of Vibration, Temperature and Speed Measurements for Multiple Types of Localized Defects on Spherical Roller Bearings across Multiple Operating Conditions*. Zenodo. doi: 10.5281/ZENODO.13913254

Giraud, L., Di Maggio, L. G., Giorio, L., & Delprete, C. (2025, April). Dynamic Multibody Modeling of Spherical Roller Bearings with Localized Defects for Large-Scale Rotating Machinery. *Sensors*, 25(8), 2419. doi: 10.3390/s25082419

Lei, Y., He, Z., Zi, Y., & Hu, Q. (2007, July). Fault diagnosis of rotating machinery based on multiple ANFIS combination with GAs. *Mechanical Systems and Signal Processing*, 21(5), 2280–2294. doi: 10.1016/j.ymsp.2006.11.003

Lei, Y., Jia, F., Lin, J., Xing, S., & Ding, S. X. (2016). An Intelligent Fault Diagnosis Method Using Unsupervised Feature Learning Towards Mechanical Big Data. *IEEE Transactions on Industrial Electronics*, 63(5), 3137–3147. (Publisher: IEEE) doi: 10.1109/TIE.2016.2519325

Lei, Y., Yang, B., Jiang, X., Jia, F., Li, N., & Nandi, A. K. (2020). Applications of machine learning to machine fault diagnosis: A review and roadmap. *Mechanical Systems and Signal Processing*, 138, 106587. (Publisher: Elsevier Ltd) doi: 10.1016/j.ymsp.2019.106587

Liu, C., & Gryllias, K. (2022, September). Simulation-Driven Domain Adaptation for Rolling Element Bearing Fault Diagnosis. *IEEE Transactions on Industrial Informatics*, 18(9), 5760–5770. doi: 10.1109/TII.2021.3103412

Liu, X., Liu, S., Xiang, J., & Sun, R. (2023, September). A transfer learning strategy based on numerical simulation driving 1D Cycle-GAN for bearing fault di-

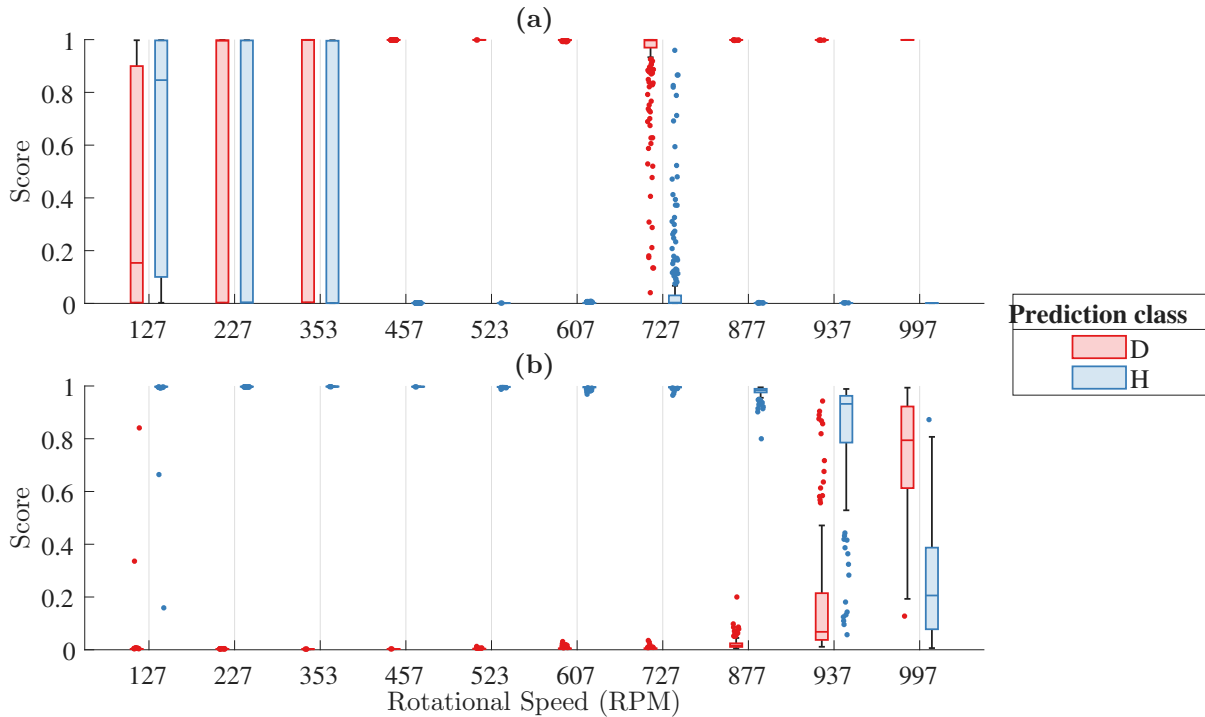


Figure 6. Prediction scores for Damaged (a) and Healthy (b) samples, at different rotational speeds of the magnetic field of the motor.

agnosis. *Information Sciences*, 642, 119175. doi: 10.1016/j.ins.2023.119175

McFadden, P., & Smith, J. (1984). Model for the vibration produced by a single point defect in a rolling element bearing. *Journal of Sound and Vibration*, 96(1), 69–82. doi: 10.1016/0022-460X(84)90595-9

Misbah, I., Lee, C., & Keung, K. (2024, January). Fault diagnosis in rotating machines based on transfer learning: Literature review. *Knowledge-Based Systems*, 283, 111158. doi: 10.1016/j.knosys.2023.111158

Pan, S. J., & Yang, Q. (2010). A Survey on Transfer Learning. *IEEE Transactions on Knowledge and Data Engineering*, 22(10), 1345–1359. (Publisher: IEEE ISBN: 9789811559709) doi: 10.1109/TKDE.2009.191

Smith, W. A., & Randall, R. B. (2015). Rolling element bearing diagnostics using the Case Western Reserve University data: A benchmark study. *Mechanical Systems and Signal Processing*, 64-65, 100–131. (Publisher: Elsevier) doi: 10.1016/j.ymsp.2015.04.021

Sobie, C., Freitas, C., & Nicolai, M. (2018). Simulation-driven machine learning: Bearing fault classification. *Mechanical Systems and Signal Processing*, 99, 403–419. (Publisher: Elsevier Ltd) doi: 10.1016/j.ymsp.2017.06.025

Surucu, O., Gadsden, S. A., & Yawney, J. (2023, July). Condition Monitoring using Machine Learning: A Review of Theory, Applications, and Recent Advances. *Expert Systems with Applications*, 221, 119738. doi:

10.1016/j.eswa.2023.119738

Tang, S., Ma, J., Yan, Z., Zhu, Y., & Khoo, B. C. (2024, August). Deep transfer learning strategy in intelligent fault diagnosis of rotating machinery. *Engineering Applications of Artificial Intelligence*, 134, 108678. doi: 10.1016/j.engappai.2024.108678

Traganitis, P. A., & Strangas, E. G. (2023, August). Perspectives of Transfer Learning on the Diagnosis of Faults in Electrical Machines, Power Electronics, and Drives. In *2023 IEEE 14th International Symposium on Diagnostics for Electrical Machines, Power Electronics and Drives (SDEMPED)* (pp. 535–541). Chania, Greece: IEEE. doi: 10.1109/SDEMPED54949.2023.10271469

Vehviläinen, M., Tahkola, M., Keränen, J., El Bouharrouti, N., Rahkola, P., Halme, J., ... Belahcen, A. (2024, September). 3D Multibody Simulation of Realistic Rolling Bearing Defects for Fault Classifier Development. In *2024 International Conference on Electrical Machines (ICEM)* (pp. 1–7). (ISSN: 2473-2087) doi: 10.1109/ICEM60801.2024.10700332

Wang, D., Tse, P. W., & Tsui, K.-L. (2013, February). An enhanced Kurtogram method for fault diagnosis of rolling element bearings. *Mechanical Systems and Signal Processing*, 35(1-2), 176–199. (Publisher: Academic Press) doi: 10.1016/J.YMSSP.2012.10.003

Wang, T., Chen, L., Lu, H., Wang, S., Li, Z., Zhang, W., & Mei, J. (2023, June). Finite Element Dynamic Model

and Vibration Signal Simulation of Rolling Bearing With Local Faults. In *Volume 2: Manufacturing Equipment and Automation; Manufacturing Processes; Manufacturing Systems; Nano/Micro/Meso Manufacturing; Quality and Reliability* (p. V002T06A033). New Brunswick, New Jersey, USA: American Society of Mechanical Engineers. doi: 10.1115/MSEC2023-105504

Widodo, A., & Yang, B.-S. (2007, August). Support vector machine in machine condition monitoring and fault diagnosis. *Mechanical Systems and Signal Processing*, 21(6), 2560–2574. (Publisher: Academic Press) doi: 10.1016/J.YMSSP.2006.12.007

Zhao, C., Zhang, Q., Wang, C., & Peng, H. (2023, June). Digital twin based bearing fault simulation modeling strategy and display dynamics. In *2023 6th International Symposium on Autonomous Systems (ISAS)* (pp. 1–5). Nanjing, China: IEEE. doi: 10.1109/ISAS59543.2023.10164348

Zhou, J., Zheng, L.-Y., Wang, Y., & Gogu, C. (2020). A Multistage Deep Transfer Learning Method for Machinery Fault Diagnostics Across Diverse Working Conditions and Devices. *IEEE Access*, 8, 80879–80898. doi: 10.1109/ACCESS.2020.2990739

Zhu, Z., Wang, L., Peng, G., & Li, S. (2021, June). WDA: An Improved Wasserstein Distance-Based Transfer Learning Fault Diagnosis Method. *Sensors*, 21(13), 4394. doi: 10.3390/s21134394

BIOGRAPHIES



Luca Girardo received the M.S. degree in Mechanical Engineering from Politecnico di Torino, Turin, Italy, in 2024, with a thesis on multibody simulation of damaged spherical roller bearings for fault detection. In 2025, he started his Ph.D. in Mechanical Engineering at the Department of Mechanical and Aerospace Engineering (DIMEAS),

Politecnico di Torino, within the Industrial Systems Engineering and Design research group. His current research interests include experimental and numerical modeling of rotating machinery, with a focus on large bearings and rotor systems, as well as the development of efficient condition monitoring and predictive maintenance strategies. He works on multibody modeling, signal processing, and data-driven fault detection, integrating simulation and experimental data to improve the reliability and maintainability of industrial systems.



Luigi Gianpiero Di Maggio received the M.S. degree in Mechanical Engineering in 2019 and the Ph.D. degree in Mechanical Engineering from Politecnico di Torino, Turin, Italy, in 2023. His doctoral research activity focused on the application of Ar-

tificial Intelligence techniques to fault detection and predictive maintenance of rotating systems. From 2023 to 2024, he was a Research Assistant with the Department of Mechanical and Aerospace Engineering (DIMEAS), Politecnico di Torino, working on synthetic data generation using generative models, advanced time-series analysis for condition monitoring, and the application of Large Language Models (LLMs) to industrial data analysis. Since 2024, he has been a fixed-term Assistant Professor at DIMEAS. His current research interests include predictive maintenance, generative AI, anomaly detection, and the integration of AI agents and Large Language Models (LLMs) tools into industrial diagnostic and monitoring workflows, with a strong focus on data-driven methods for rotating machinery.



Eugenio Brusa received the degree in Aeronautical Engineering, in 1993, and the Ph.D. degree from Politecnico di Torino, Turin, Italy, in 1997. Since 1998, he has held several academic positions, first as a Researcher, then as an Associate Professor (2002), and, since 2013, as a Full Professor. His career has included appointments

at the University of Udine (2001–2008) and at Politecnico di Torino (1998–2001; 2008–present). He has served as Technical Director of the Master’s Program in ‘Project Management and System Engineering’ (2007–2008), Coordinator of the Mechanical Engineering Program (2015–2018), and Director of the Doctoral School (2018–2024). His research interests include structural mechatronics, dynamic design of machines, rotors and industrial systems in aerospace, steel and ground-vehicle applications, as well as systems engineering methodologies and tools for industrial, European, and regional projects. He has contributed to the establishment of several research laboratories at Politecnico di Torino, including the Mechatronics Laboratory (1993), the Testing and Characterization of Rotating Systems Laboratory (1997), and the Industrial Systems Engineering and Design Laboratory (2020). He is the author of numerous conference and journal papers and three monographs.



Cristiana Delprete received the degree in Mechanical Engineering from Politecnico di Torino, Turin, Italy, in 1988 and the Ph.D. degree in Applied Mechanics, Mechanical Systems, and Structures in 1993. She was a Researcher at Politecnico di Torino from 1991 to 1998, an Associate Professor from 1998 to 2017, and has been a Full Professor

since 2017. She co-founded the Interdepartmental Mechatronics Laboratory at Politecnico di Torino, serving as its Technical Coordinator from 1993 to 1996, and led the research group ‘Design of Powertrain and Engine Components: Materials, Testing, and Simulation’ from 2001 to 2020 within

DIMEAS. Since 2009, she has been the University Advisor for the Policumbent Student Team, and since 2005, she has been an active member of SAE International. She is co-founder and co-leader of the Industrial Systems Engineering and Design Laboratory (2020) at Politecnico di Torino. Her research interests include the design, testing, and simulation of powertrain and mechanical components, with emphasis on materials, durability, and advanced experimental methodologies.

APPENDIX

Table 4 reports the time and frequency domain features used to create the datasets from the acceleration time signals. In this work, x indicates the sample acceleration signal, the suffix n specifies the discrete time instant and N the number of discrete instants in a sample. S_x is the Fast Fourier Transform of a sample, suffix k is the indicator of the discrete frequency and K the total spectral length.

Time domain	Frequency domain
$\bar{x} = \frac{\sum_{n=1}^N x_n}{N} = E(x)$	$\bar{S}_x = E(S_x)$
$STD(x) = \sqrt{\frac{1}{N-1} \sum_{n=1}^N (x_n - \bar{x})^2}$	$\frac{1}{K-1} \sum_{k=1}^K (S_{x,k} - \bar{S}_x)^2$
$MSAR(x) = E(\sqrt{ x })^2$	$\frac{E[(S_x - \bar{S}_x)^3]}{STD^3(S_x)}$
$RMS(x) = \sqrt{E(x_n^2)}$	$\frac{E[(S_x - \bar{S}_x)^4]}{STD^4(S_x)}$
$P_{max}(x) = \max(x)$	$FC = \frac{E[f_x \cdot S_x]}{E[S_x]}$
$\frac{E((x_n - \bar{x})^3)}{STD^3(x)}$	$SD = \sqrt{\frac{E[(f_x - FC)^2] \cdot S_x}{E[S_x]}}$
$\frac{E((x_n - \bar{x})^4)}{STD^4(x)}$	$\sqrt{\frac{E[f_x^2 \cdot S_x]}{E[S_x]}}$
$\frac{P_{max}}{RMS(x)}$	$\sqrt{\frac{E[f_x^4 \cdot S_x]}{E[f_x^2 \cdot S_x]}}$
$\frac{P_{max}}{MSAR}$	$\sqrt{\frac{E[f_x^2 \cdot S_x]}{\sqrt{E[f_x^4 \cdot S_x] \cdot E(S_x)}}}$
$\frac{P_{max}(x)}{E(x)}$	$\frac{SD}{FC}$
$\frac{RMS(x)}{E(x)}$	$\frac{E[(f_x - FC)^3 \cdot S_x]}{SD^3}$
	$\frac{E[(f_x - FC)^4 \cdot S_x]}{SD^4}$

Table 4. Features used as the dataset predictors.